WATER RESOURCES RESEARCH, VOL. 49, 202–215, doi:10.1029/2011WR011789, 2013

Three-dimensional flow in centered pool-riffle sequences

José F. Rodríguez,[1] Carlos M. García,[2,3] and Marcelo H. García[4]

Received 23 December 2011; revised 16 November 2012; accepted 21 November 2012; published 16 January 2013.

[1] Pool-riffle sequences are geomorphological features of many streams, thought to contribute to the hydrodynamic variability necessary to support healthy habitat conditions. Due to this fact, the addition of artificial pools and riffles is a common alternative for restoration projects on channelized streams. In this paper, detailed three-dimensional (3-D) flow measurements conducted on a scale model of an existing pool-riffle design implemented as part of a restoration project is presented. The design incorporated the basic features of natural pool-riffle sequences but maintained the deepest part of the pool in the center of the cross section and away from the banks. Results showed that the 3-D flow patterns were qualitatively different for two discharge conditions tested. The lower discharge case was strongly affected by the topography, displaying a pattern consistent with a secondary flow generated by the curvature of the streamlines. The higher discharge case was less affected by the topography, presenting a secondary flow pattern similar to that observed over a flat bed and typically associated with turbulence anisotropy. Self-maintenance and flow variability were also investigated. Even though convergence of the values of bed shear stresses at pool and riffle sections with increasing discharge did take place, reversal conditions did not occur. The difference in flow structure with flow stage was also reflected in the spatial flow variability, the lower discharge displaying larger variability than the higher discharge. The higher discharge generated a level of variability comparable with the values obtained over a flat bed.

Citation: Rodríguez, J. F., C. M. García, and M. H. García (2013), Three-dimensional flow in centered pool-riffle sequences, *Water Resour. Res.*, *49*, doi:10.1029/2011WR011789.

1. Introduction

[2] Pools and riffles are geomorphological features ubiquitously found in straight, meandering, and braiding river systems. They are considered a basic component of a universal unit-bar structure, which interacts with the planform and flow field to generate a characteristic bed topography [*Dietrich*, 1987]. They have also been regarded as essential elements in the initiation and development of meandering [*Thompson*, 1986; *Rhoads and Welford*, 1991]. In later years, it has been realized that their hydrodynamic variability provides a variety of habitat conditions required for different fish species and for the same species at different stages of its life. This last point has made the addition of artificial pools and riffles a very common alternative for restoration projects on channelized streams [*Newbury and Gaboury*, 1993; *Rodríguez et al*., 2000; *Rhoads et al*., 2011].

[3] Natural pools and riffles are typically arranged in sequence, often displaying pools with a skewed shape in which the deepest point alternates from one side of the cross section to the other. The skewness alternation is characteristic of meandering streams and it has been linked to bank erosion and subsequent meander development [*Rhoads and Welford*, 1991]. Due to this fact, artificial pools and riffles resembling skewed natural sequences may not be suitable for stream restoration projects in heavily populated areas with infrastructure encroached floodplains.

[4] This was the case in the restoration of the North Branch of the Chicago River (WFNBCR) at Northbrook, Illinois, a project that included the design, testing, and construction of centered pool-riffle structures aimed at increasing flow variability of a channelized urban stream without compromising the stability of the banks [*Rodríguez et al*., 2000; *Wade et al*., 2002; *Rhoads et al*., 2008, 2011]. An experimental program was carried out to investigate the three-dimensional (3-D) flow structure of pools and riffles in support of the design process and included four different bed configurations with increasing levels of hydrodynamic complexity: flat bed, centered pool-riffles, alternate pool-riffles, and alternate pool-riffles with vegetation [*Rodríguez*, 2004; *Rodríguez and García*, 2008; *López*, 2006]. The sequence can also be seen as different steps in the restoration process, starting on a flat-bed degraded stream with no

[1]Civil, Surveying and Environmental Engineering, School of Engineering, University of Newcastle, Callaghan, New South Wales, Australia.
[2]Centro de Estudios y Tecnología del Agua, Facultad de Ciencias Exactas, Físicas y Naturales, Universidad Nacional de Córdoba, Córdoba, Argentina.
[3]Consejo Nacional de Investigaciones Científicas y Técnicas (CONICET), Buenos Aires, Argentina.
[4]Ven Te Chow Hydrosystems Laboratory, Department of Civil and Environmental Engineering, University of Illinois at Urbana-Champaign, Urbana, Illinois, USA.

Corresponding author: J. F. Rodríguez, Civil, Surveying and Environmental Engineering, School of Engineering, University of Newcastle, Callaghan, NSW 2308, Australia. (jose.rodriguez@newcastle.edu.au)

0043-1397/13/2011WR011789

geomorphologic diversity and finishing on a more natural system with pool-riffle structures and established vegetation. *Rodríguez and García* [2008] conducted experiments over a flat rough bed representing the channelized stream or prerestoration condition. The present paper focuses on the results of the centered pool-riffle (CPR) experiments using the same facility and similar setup and bed material than the ones used in *Rodríguez and García* [2008], thus, their results constitute the ideal background for comparison. As the restoration of the channelized stream was based on the addition of variability in the flow patterns through the construction of pools and riffles, the focus of this study was on the evaluation of the 3-D structure of the flow and the quantification of the hydrodynamic variability of this particular pool-riffle design.

2. Hydrodynamics of Pool-Riffle Sequences

[5] An important issue to address within the study was the long-term stability of the pool-riffle design, which is closely linked to its hydrodynamic behavior. In particular, it was of interest to investigate whether the structures were able to self-maintain in the way natural pool-riffle sequences do. Although a complete and thorough explanation for pool-riffle self-maintenance is yet to be formulated, there are a number of flow and sediment mechanisms that have been identified as key to the remarkable consistency of this bedform morphology observed in nature under a wide variety of flow and substrate conditions. A very important characteristic of pools and riffles is that their hydrodynamic behavior depends on discharge: velocities over riffles are faster than in pools for most discharges due to the riffles being shallower [*Clifford and French*, 1993]; however, for high discharges, the flow is much more uniform, attenuating the differences between pool and riffle velocities. In some instances, a reversal in velocity can occur, with pool velocities surpassing riffle velocities at or above bankfull flow. This fact was first observed by *Gilbert* [1914] and later used by *Keller* [1971, 1972] to explain the self-maintenance of pool-riffle sequences. According to the velocity-reversal hypothesis, higher pool velocities are necessary at some stage to entrain the material accumulated during previous flows and to deposit it on the riffles. There is evidence to both support [*Andrews*, 1979; *Keller*, 1971; *Lisle*, 1979; *O'Connor et al*., 1986; *Petit*, 1987] and refute [*Bathurst*, 1982; *Bhowmik and Demissie*, 1982; *Teleki*, 1972; *Sear*, 1996] the reversal hypothesis. Although the original velocity-reversal research focused on near-bed conditions [*Keller*, 1971, 1972], it has also been extended to cross-sectional averaged conditions, mostly for practical reasons. This simplification implies the assumption of a logarithmic velocity profile and relatively minor variations in the cross-sectional velocity distribution, which may not apply to all situations [*Thompson*, 2011]. For the reversal hypothesis to hold in a cross-sectional average sense, flow continuity requires the cross-sectional area of the pool to be larger than that of the riffle for low discharges, and the opposite to occur for high discharges [*Lane and Borland*, 1954]. It is not unusual for natural rivers to have pools with an approximate triangular shape (wetted area increases with the second power of the depth) and riffles with an approximate rectangular shape (wetted area increases linearly with depth), in which case velocity reversal can occur. Channels with wall constrictions, like urban streams or laboratory flumes, have more limitations fulfilling this requirement.

[6] Very few measurements of the actual velocity reversal exist due to the difficulty of measuring during high discharges; in most cases, it has been inferred, deduced, or computed using additional assumptions. Alternative or complementary explanations for maintenance focus on the different characteristics of the bed material and near-bed flow conditions, which do not necessarily follow the cross-sectional average flow trends. Issues like armoring, imbrication, packing density, and microtopography may reduce the mobility of the riffle making it more resistant to erosion than the pool [*Clifford*, 1993; *Sear*, 1996], whereas flow concentration due to constrictions and associated turbulent coherent structures can enhance the scouring of pools [*MacVicar and Roy*, 2007a, 2007b; *Thompson and Wohl*, 2009]. Coherent structures seem to operate differently in pools than in riffles [*Clifford*, 1993; *Clifford and French*, 1993] and may create instantaneous conditions for sediment transport before the entrainment threshold is reached by the time-averaged variables [*Nelson et al*., 1993, 1995]. These local 3-D flow and turbulent effects can produce near-bed self-maintenance conditions even if average flow variables do not [*Thompson*, 2011; *MacWilliams et al*., 2006; *Caamaño et al*., 2012], particularly when sediment dynamics is considered. Coupling of flow and sediment dynamics in a simple one-dimensional framework has also shown that pool-riffle self-maintenance can occur well before velocity reversal [*de Almeida and Rodríguez*, 2011, 2012]. Analysis of the coupled flow and sediment dynamics in a full 3-D, unsteady framework would certainly shed light on the most important mechanisms for self-maintenance; however, this has not been done to date. From a practical perspective, it seems that an equalization of flow conditions in pools and riffles during high discharges combined with other mechanisms related to sediment mobility, including 3-D and turbulence flow effects, can be enough to maintain a stable morphology over the long term.

[7] Mainly due to its implications for geomorphic self-maintenance and to a lesser extent also due to its importance for ecological variability, the 3-D hydrodynamics of pools and riffles has received some attention in the past. Previous research has shown that transverse velocity vectors indicate lateral divergence over the riffles and lateral convergence over the pools due to successive contractions and expansions of the flow from narrow pools to wide riffles [*Keller*, 1972; *MacVicar and Roy*, 2007]. The term lateral divergence/convergence is used in this paper to describe spatial transverse velocity patterns to avoid confusion with the use of the term convergence to describe the equalization of flow variables with increasing discharge. The alternation of lateral convergence and divergence along the thalweg is associated with a characteristic pattern of secondary circulation with surface convergent/near-bed divergent twin cells at the pool center and surface divergent/near-bed convergent cells at the riffle center (Figure 1) [*Thompson*, 1986; *Clifford and Richards*, 1992; *MacWilliams et al*., 2006; *Rhoads et al*., 2008], which is different from patterns in meandering streams. The near-bed divergent flow at the bottom of pools is thought to contribute to the removal of sediments and thus to the self-maintenance of the pool-riffle unit. The three dimensionality of the flow not only manifests itself in the form of secondary circulation but also includes effects on

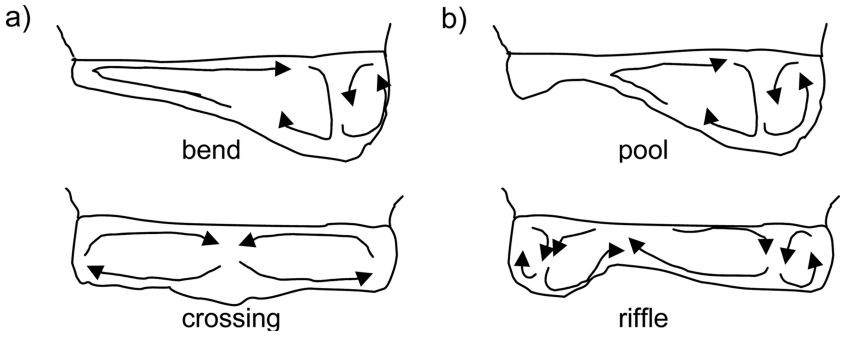

Figure 1. Secondary flow induced by streamline curvature: (a) meandering thalweg and (b) pool-riffle sequence (adapted from *Thompson*, 1986).

the distribution of the streamwise velocity. Zones of flow concentration or jetting not directly associated with obstacles have been reported in pool-riffle sequences [*Keller*, 1971; *Clifford and Richards*, 1992; *MacWilliams et al*., 2006; *Caamaño et al*., 2012], and their distinct behavior under different discharge conditions has been linked to self-maintenance. It is not totally clear how habitat characteristics are influenced by 3-D flow dynamics and its variability, although it is recognized that local rather than averaged flow measurements are required to assess physical habitat conditions [*Hart and Finelli*, 1999; *Nikora et al*., 2002].

[8] Links to geomorphological and ecological processes in pool-riffle sequences can be addressed only partially using cross-sectional or depth-averaged hydrodynamic information. To date, most descriptions of 3-D flow in pools and riffles have been attempted using numerical simulations [*Booker et al*., 2001; *Cao et al*., 2003; *MacWilliams et al*., 2006; *Caamaño et al*., 2012]. A limited number of laboratory measurements on pools and riffles have been carried out; however, they have used a simplified geometric description [*Thompson et al*., 1999; *Thompson*, 2002]. This paper presents detailed laboratory flow measurements that allow for the reconstruction of 3-D flow patterns in a pool-riffle design that aims to provide a level of flow variability similar to what would be expected in a natural stream. Although these measurements strictly apply to the specific design tested, they can also provide insight into some of the basic geomorphological and ecological properties of pool-riffle sequences observed in nature. The measurements presented in this paper have been conducted on a scale model of an existing pool-riffle design implemented as part of the aforementioned restoration project [*Wade et al*., 2002; *Rhoads et al*., 2008, 2011]. The design incorporates some of the important features of natural pool-riffle sequences, like wide shallow riffles and narrow deep pools with a smooth transition. The data gathered are thus relevant in terms of representativeness and resolution and have the potential to become a testing set for numerical models before application to more natural settings, in which richer 3-D flow and turbulence patterns (including flow separation and associated turbulent coherent structures) are likely to play a role.

3. Equipment and Methods

[9] A tilting flume 12.20 m long, 0.91 m wide, and 0.6 m high was used for the experiments. The flume received a constant supply of water from a head tank and had an adjustable downstream gate to regulate the flow depth. A fixed, hydraulically rough, uneven bed comprising three riffles and three pools was built using commercial 3/8″ crushed stone chips ($D_{90} = 1$ cm, $D_m = 0.57$ cm, and grain standard deviation $\sigma_g = 0.20$ cm; Figures 2 and 3). The design of the centered pool-riffle sequence followed some basic geomorphological characteristics of natural pool-riffle sequences, including narrow pools and wide riffles, a gradual pool-riffle transition, and a longitudinal spacing between riffles (or pools) of five times the stream width [*Keller and Melhorn*, 1978]. The longitudinal profile along the centerline of the design was defined by a sinusoidal

Figure 2. Centered pool-riffle sequence built using 3/8″ stone chips. Note the location of guiding cross sections with smaller spacing in the pool.

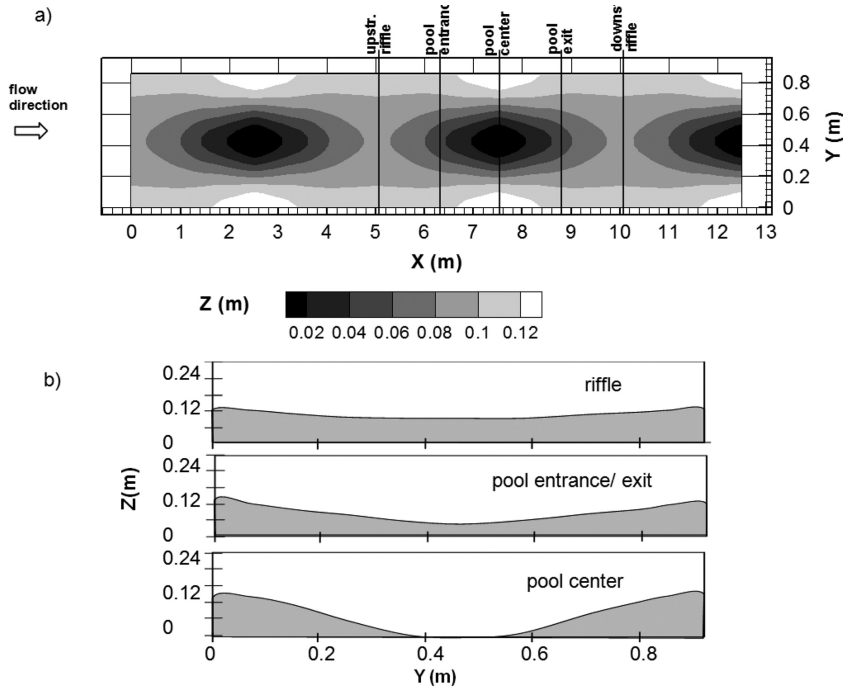

Figure 3. Bed topography and measurement sections: (a) plan view and (b) selected cross sections.

curve, and the cross sections were obtained using third-order polynomials. When applied to the conditions of the WFNBCR at Northbrook, the dimensions of the experimental pool-riffle sequence correspond to a 1:7 scaling.

[10] Shaping of the bed was guided by cross-sectional metal templates separated 1 m in the riffle areas and 0.5 m in the pool areas (Figure 2), resulting in the topography shown in Figure 3. The origin of a global orthogonal streamwise (X), spanwise (Y), and bed-normal (Z) coordinate system with respect to the overall channel slope S_0 of 0.25% was defined at the beginning of the sediment layer on the left wall and at the elevation of the deepest point in the central pool (i.e., the channel centerline). Because the bed was uneven, the orientation of the spanwise and bed-normal directions varied at each point, and local boundary-layer type coordinates x, y, and z were also used.

[11] The experimental setup was completed with point gauges for water surface measurements and a downlooking 3-D Sontek microacoustic Doppler velocimeter (ADV) for flow velocity measurements. The micro-ADV was operated at a sampling rate of 25 Hz over a 90 mm^3 sampling volume. Orientation was done so that the instrument's z coordinate coincided with the vertical projections and the x and y coordinates were aligned with the horizontal projections of the streamwise (X) and spanwise (Y) channel coordinates, respectively. Due to minimum depth requirements of the sensor, the upper 6 cm of the flow could not be measured. Velocities were measured in the central pool-riffle unit at five cross sections 1.25 m apart: upstream riffle (X = 5.05 m), pool entrance (X = 6.30 m), pool center (X = 7.55 m), pool exit (X = 8.80 m), and downstream riffle (X = 10.05 m; Figure 3). At each cross section, measurements were carried out on one half of the cross section with a spacing of 5 and 1 cm in the spanwise and vertical directions, respectively. Preliminary tests verified flow symmetry with respect to the centerline of the cross section [*Rodríguez et al.*, 2001]. Water surface elevations were measured at several points along the channel centerline only, as the transverse variations on the water surface were too small to be measured accurately.

[12] The notation for the velocity vector components in the X (streamwise), Y (spanwise), and Z (bed-normal) directions are U, V, and W, respectively, for the Reynolds-averaged local velocities; u, v, and w for the turbulent velocity fluctuations and u', v', and w' for the root mean square value of the velocity fluctuations. Overbars are used for time averaging (except for U, V, and W), and brackets $\langle\rangle$ are used for spatial averaging over the pool-riffle unit. A summary of the experimental conditions is presented in Table 1, which also includes information on previous experiments over a flat bed [*Rodríguez and García*, 2008]. In Table 1, Q is the discharge, $\langle U\rangle$ is the mean streamwise velocity averaged

Table 1. Comparison Between Previous and Current Experiments (Reach-Average Values)

Reference	Q (m^3/s)	$\langle h\rangle$ (m)	$\langle U\rangle$ (m/s)	$\langle U^*\rangle$ (m/s)	Re ($\times 10^3$)	Fr	$\langle k_s^+\rangle$
Rodríguez and García [2008], experiment FB1	0.05	0.11	0.48	0.047	44	0.45	470
Rodríguez and García [2008], experiment FB2	0.1	0.15	0.72	0.053	82	0.6	530
This paper, experiment CPR1	0.03	0.09	0.37	0.045	30	0.38	450
This paper, experiment CPR2	0.11	0.19	0.64	0.059	90	0.47	590

over the whole pool-riffle unit, $\langle U^* \rangle = (g\langle R_h \rangle \langle S_w \rangle)^{1/2}$ is the pool-riffle unit streamwise shear velocity, with g, $\langle R_h \rangle$, and $\langle S_w \rangle$ being the gravitational acceleration, the unit-averaged hydraulic radius, and the unit-averaged water surface slope, respectively; $Re = \langle U \rangle \langle R_h \rangle / \nu$ is the bulk Reynolds number, with ν denoting kinematic viscosity of water; $Fr = \langle U \rangle / (g\langle h \rangle)^{1/2}$ is the Froude number, with $\langle h \rangle$ standing for the unit-averaged hydraulic depth; $\langle k_s^+ \rangle = k_s \langle U^* \rangle / \nu$ is the unit-averaged dimensionless roughness, with k_s representing the bed roughness (set equal to D_{90} for the present computations). All the experiments reported in Table 1 have a longitudinal average bed slope S_0 of 0.25%, as already noted.

[13] Two flow conditions were tested, with discharges of 0.03 (CPR1) and 0.11 (CPR2) m^3/s. The low and high discharges resulted from converting to a 1:7 Froude scale the 1 and 2 year return-period floods for the WFNBCR at Northbrook, Illinois, respectively. The 2 year return flood was used as this value is often associated to geomorphologic changes in rivers. The low discharge, on the other hand, was the shallower flow condition that allowed for a good flow measurement strategy, given the equipment available. It must be noted, however, that in a real stream the 1 year return flow is not necessarily a low discharge. Similar flow conditions have been tested in the same setup over a flat bed [*Rodríguez and García*, 2008], which provide important background information. Table 1 shows that in both experiments the bed was hydraulically rough, with values of $\langle k_s^+ \rangle$ well above 70 [*Nezu and Nakagawa*, 1993], and the flow was turbulent and subcritical. Each velocity point was sampled for at least 120 s. This record length ensured convergence in the values of the mean and first-order statistics of the velocity time series [*Rodríguez and García*, 2008]. Due to the unevenness of the bed, local flow conditions were strictly non uniform. Over the central pool-riffle unit, the flow was uniform in an average sense, as the average slope of the water surface $\langle S_w \rangle$ was parallel to the slope of the flume S_0 and the boundary layer was not affected by the flume entrance conditions. This was verified by comparing velocity profiles at the centers of the upstream and downstream riffles, which showed no substantial changes in the velocity distributions with the streamwise direction.

[14] Shear velocities were computed using the law of the wall, which required a transformation from global (X, Y, Z) to local (x, y, z) boundary-layer coordinates along bed-normal rays. The law of the wall for hydraulically rough conditions was used with a value of $\kappa = 0.4$.

$$\frac{U}{U^*} = \frac{1}{\kappa} \ln\left(\frac{z}{k_s}\right) + 8.5. \tag{1}$$

[15] In a strict sense, a boundary-layer analysis (with no transverse shear) over an irregular cross section only applies along rays that are perpendicular to the isovels; however, the velocity profile along these rays is not logarithmic, and the problem requires a numerical solution [*Shimizu*, 1989]. *Lundgren and Jonsson* [1964] proposed neglecting lateral shear and using a logarithmic profile along bed-normal rays, which is an acceptable approximation for rectangular and trapezoidal channels [*Pizzuto*, 1991] and cross sections with small lateral bed curvature [*Parker*, 1978]. In the present experiments, the maximum lateral bed curvature occurred at the pools, with a value of approximately 1.7 m^{-1}, but was considerable lower, i.e., less than 0.3 m^{-1}, for the rest of the cross sections analyzed. It was assumed for the analysis of the velocity data that a bed-normal boundary layer approach was valid.

[16] The coordinate transformation procedure involved manipulations to the original data, including interpolations and axis rotations, which were carried on with the help of the graphical software Tecplot. Once the data were in boundary-layer coordinates, inner scaling similarity was used to determine the shear velocity U^* by fixing $k_s = D_{90}$ and by varying the bed position ($z = 0$) until the best data fit was obtained. This procedure has given good results when applied to flat bed experiments on a similar setup using the same bed material, whose unevenness and sound-reflective properties interfere with the ADV bed positioning readings [*Rodríguez and García*, 2008]. As often done on rough irregular beds, the bed (or virtual origin for the velocity profile) was assumed to be at a distance between 0 and k_s below the top of the roughness elements (TREs) [*Smart*, 1999]. The position of the TRE at each vertical was determined manually before inundating the channel, using a 2.5 × 2.5 cm^2 metal strip on top of the stone chips (Figure 4). This level was assumed as the local TRE, and the ADV was set so that the lowest velocity measurements had their control volume placed at the TRE. This last step was done by placing a 5 cm wooden block between the metal strip and the ADV central sensor head.

[17] Strictly speaking, the use of the law of the wall only applies to steady two-dimensional uniform flows with high relative submergence (i.e., flow depth/roughness height), and therefore, the extension to situations with secondary currents, accelerations, decelerations, and uneven beds must be considered an approximation. Other methods of estimating bed shear stresses were investigated; however, they produced less reliable results. The use of the principal Reynolds stress distribution $\rho\overline{uw}$ was affected by local acceleration and deceleration, and the near-bed estimates were prone to errors as reported by *MacVicar and Rennie* [2012], *Song and Chiew* [2001], and *Yang and Chow* [2008]. The use of the local water surface slope also presented limitations in terms of accuracy.

Figure 4. Procedure used for location of the TREs and positioning of the ADV.

4. Results

[18] The three-dimensional structure of the flow is presented in Figures 5 and 6 (low discharge and high discharge, respectively) as a combined contour-vector plot, with contours for the streamwise velocity distribution and vectors for the secondary velocity field. The results are presented for each analyzed discharge condition at the cross sections, starting (from top to bottom) from upstream, i.e., upstream riffle ($X = 5.05$ m), pool entrance ($X = 6.30$ m), pool center ($X = 7.55$ m), pool exit ($X = 8.80$ m), and downstream riffle ($X = 10.05$ m). For the low-discharge case, it can be seen from Figure 5 that riffles have higher streamwise velocities than pools as expected and that they present a region with velocity concentration close to the channel axis, but slightly off center. This core moves toward the axis (or thalweg) as the flow progresses into the pool, potentially merging with the corresponding velocity core from the other side of the channel to form a unique core, which later splits into two cores again as the downstream riffle is reached. Transverse velocity vectors are less than 5% of the streamwise flow and show a complicated pattern as a result of the combined effects of lateral convergence/divergence, upwelling/downwelling, and rotating cells. Some characteristic features observed are that the location of the high-velocity cores tends to coincide with regions of strong downward vertical flow and that the flow laterally converges toward the pool and diverges toward the riffle.

[19] For the high-discharge case, the flow structure is notably different (Figure 6). The variation between pool and riffle velocities is not as pronounced, and the cross-sectional flow pattern clearly shows two high-velocity cores that remain essentially in the same relative position throughout the pool-riffle unit. The high-velocity cores coincide with downwelling regions, and the secondary velocities are less than 5% of the streamwise flow except for a marked upwelling at the riffles center. Lateral convergence and divergence patterns are indiscernible; however, secondary circulation is well defined.

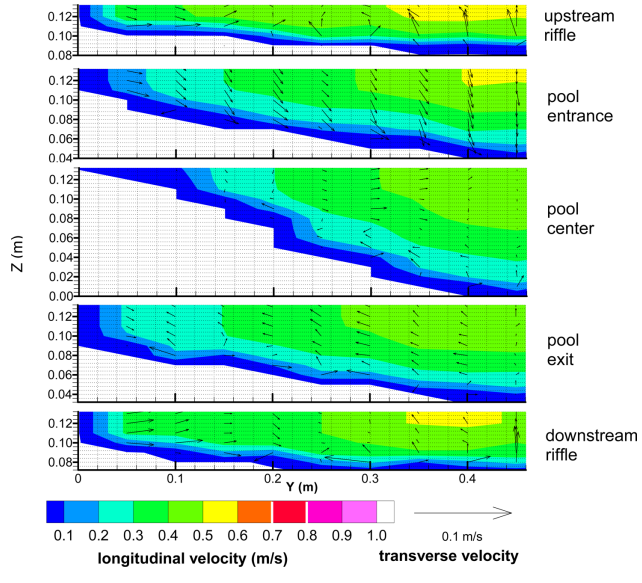

Figure 5. Three-dimensional nontransformed velocity distribution for low flow (CPR1).

[20] The recirculating cells can be more easily identified by looking at the distribution of the longitudinal vorticity Ω of Figures 7a and 7b (low discharge and high discharge, respectively). Figure 7 presents the values of Ω that have been calculated using $\Omega \equiv \partial V/\partial z - \partial W/\partial y$. According to the axis directions convention adopted in Figure 7, a cell with positive longitudinal vorticity rotates counterclockwise, whereas a negative vorticity cell rotates in the opposite direction. Combining information on the transverse velocity vector field and the streamwise vorticity, rotating cells have been sketched in Figure 7. For the low-discharge case (Figure 7a), two side-by-side elliptical cells can be observed at the riffles, which are replaced by a larger cell at the pool. The high-discharge case (Figure 7b) shows a pattern of three circulation cells, which are circular at the riffles (their width scales with the riffle depth) but stretch vertically in the pool to occupy the whole cross section.

[21] As mentioned in the section 3, bed shear velocities were obtained using the law of the wall along bed-normal rays. Bed-normal rays were defined at different Y/b positions at each cross section, with the value of Y corresponding to the bed transverse position divided by the flume width b, as shown in Figure 8. Streamwise velocity fit to the law of the wall for rough bed is shown in Figure 9, in which the velocity profiles have been dimensionalized with inner variables U^* and k_s. The U^* values have been adjusted to comply with the law of the wall along bed-normal rays on the lower 20% of the depth and k_s has been set to D_{90}. For the low-discharge case (Figure 9a), it can be observed that the streamwise velocity consistently adjusts to a logarithmic profile for all the cross sections, with a remarkable good collapse even beyond the lower 20% of the depth area. However, some shallow profiles had very few points for the logarithmic fit procedure, and therefore, the U^* values close to the channel walls must be considered with caution. Wake effects close to the surface could not be assessed due to the limitations of the ADV to measure velocities in this area of the flow. The high-discharge case (Figure 9b) reveals some minor wake effects that start to show up at distances of $z/k_s > 4$.

[22] The U^* values obtained with the law of the wall were converted to bed shear stresses $\tau = \rho U^{*2}$ and are presented in Figure 10 for the five cross sections analyzed. At each cross section, the local values have been scaled with the cross-sectional mean τ_m, obtained by integration over the wetted perimeter. To carry out the integration, the shear stresses in areas close to the walls were extrapolated by linearly continuing the observed distribution toward a value of zero at the wall. For the low-discharge case (Figure 10a), the pattern of bed shear stress consists of a superposition of oscillations on top of a more general trend. If central symmetry in the flow distribution is assumed, the general trend starts with an almost flat distribution at the riffles to then display a marked triangular shape at the pool entrance that gets wider at the pool center. The general trend is driven by the high-velocity cores and the cross-sectional shape, and there are many locations where the local peaks of the oscillations coincide with areas of strong downward vertical flow, as also reported in *Rodríguez and García* [2008] for flat-bed conditions. Bed shear stresses for the high-discharge

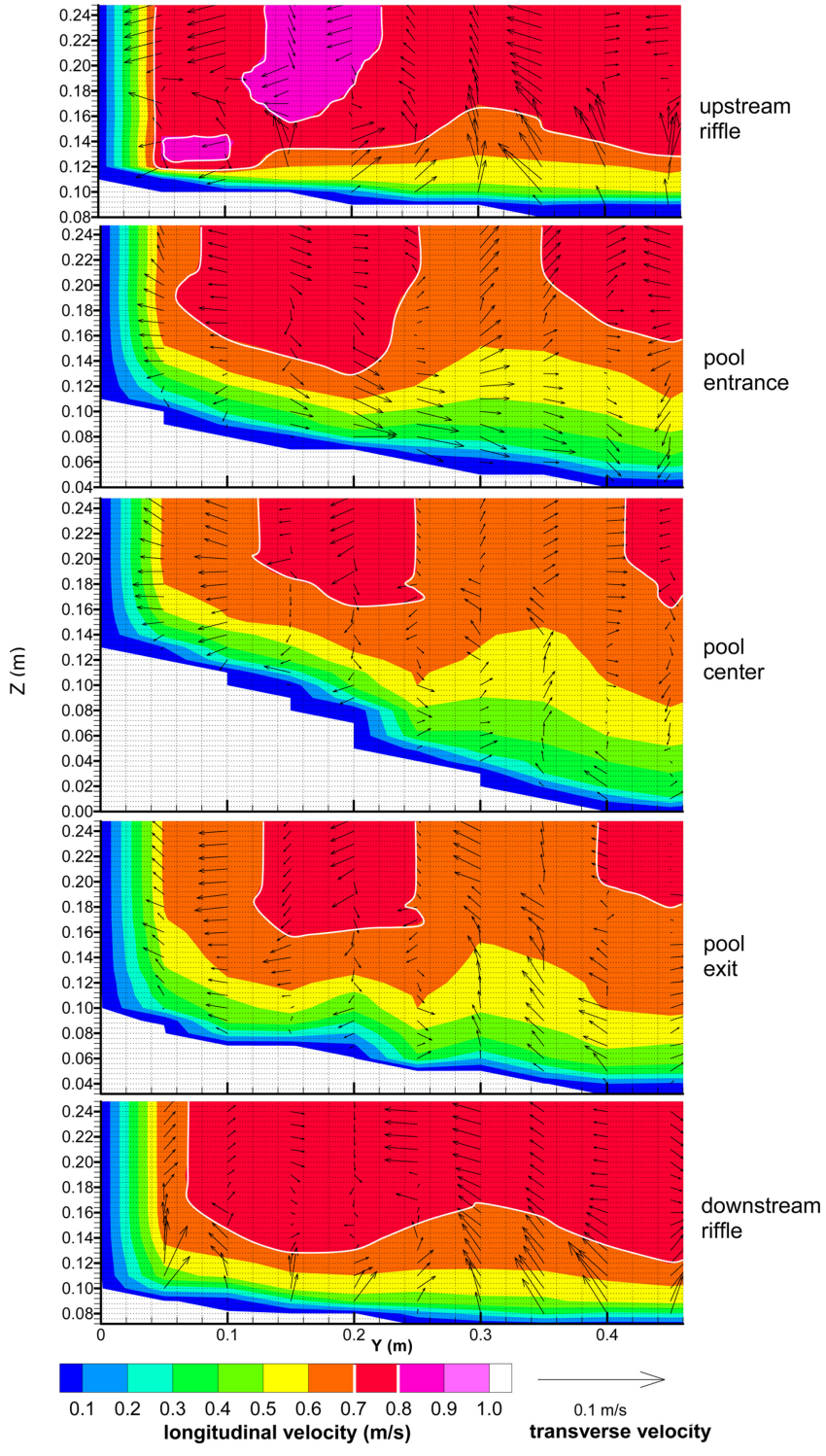

Figure 6. Three-dimensional nontransformed velocity distribution for high flow (CPR2).

case (Figure 10b) present a pattern that does not change throughout the whole unit and that is totally in phase with the downwelling and upwelling regions originated by the circulation cells. Figure 10 also includes measurements over a flat bed for similar flow discharges (FB1 and FB2 in Table 1) in which the same level of oscillations due to upwelling and downwelling associated with the circulation cells can be observed [*Rodríguez and García*, 2008].

5. Analysis and Discussion

5.1. 3-D Flow Patterns

[23] The low- and high-discharge streamwise velocities are organized around a number of high-velocity cores, also known as jets, that affect the whole 3-D flow distribution; however, their pattern is quite different in both cases. High-velocity cores have been previously observed in pool-riffle

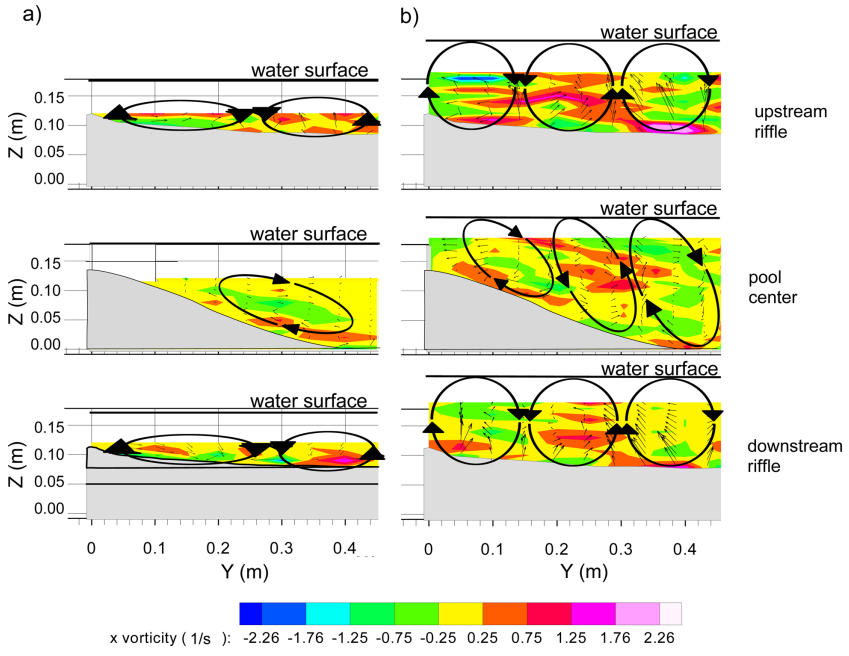

Figure 7. Cross-sectional vorticity distribution for (a) low flow (CPR1) and (b) high flow (CPR2).

sequences, particularly at pools [*Keller*, 1971; *Clifford and Richards*, 1992; *MacWilliams et al*., 2006; *Caamaño et al*., 2012] and attributed to flow contraction; however, they are also present to some extent in flat-bed situations [*Rodríguez and García*, 2008]. The low-flow pattern (Figure 5) presents one core at the riffles that moves toward the centerline at the pool. Due to the shape of the pool entrance, the core potentially consolidates with a symmetric core on the other side of the cross section at the central part of the pool, in agreement with the simulations of *MacWilliams et al.* [2006] and *Caamaño et al.* [2012]. The process is reversed toward the pool exit and downstream riffle.

[24] The analysis of time-averaged transverse velocities for the low-discharge case shows a pattern of lateral convergence at the pool entrance and lateral divergence at the pool exit, in agreement with the observations by *MacVicar and Rennie* [2012] on a straight pool. Lateral flow effects are not as strong at the pool center and at the riffles, where transverse velocities seem to indicate the presence of circulation cells. Plots of longitudinal vorticity (Figure 7) confirm the presence of two side-by-side cells at the riffles, which are elongated in the transverse direction stretching to a width of two to three times their height. The core of high velocity approximately coincides with a downwelling zones between cells at about one fourth the width. At the pool, a surface-convergent cell occupies most of the half cross section, and the velocity core coincides with a downwelling zone at the thalweg. The described behavior agrees with observations of secondary circulation cells in natural pool-riffle sequences (Figure 1) [*Thompson*, 1986]. In particular, it explains the frequently observed phenomenon of the cells inverting their rotation from surface divergent at the riffles to surface convergent at the pools [*Rhoads et al*., 2008]. The rearrangement of the cells is driven by a lateral displacement of the velocity core toward the center of the pool, the core always coinciding with a downwelling zone. Redistribution of momentum and energy by the cell at the pool is restricted to the deeper zone, having little effect on the longitudinal velocity distributions. At the riffles, however, the central upwelling seems to be effective in pushing low-momentum fluid away from the bottom and into the water column contributing to the displacement of the velocity core away from the centerline.

[25] In contrast with the low-discharge pattern, the high-discharge pattern (Figure 6) presents two cores of high streamwise velocity that do not seem to be affected by the

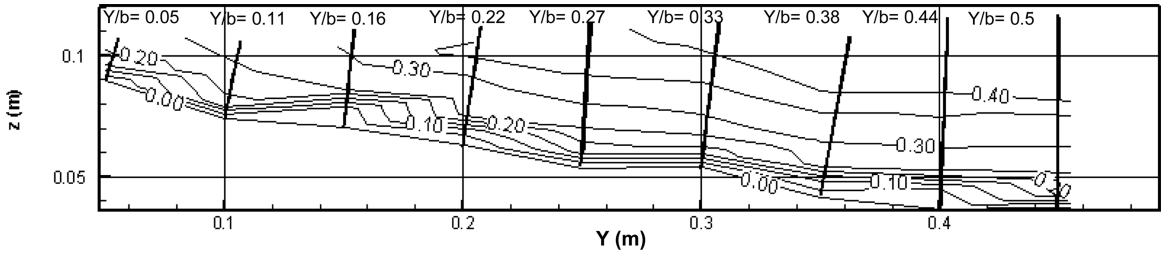

Figure 8. Establishment of bed-normal rays at the pool exit cross section for CPR1.

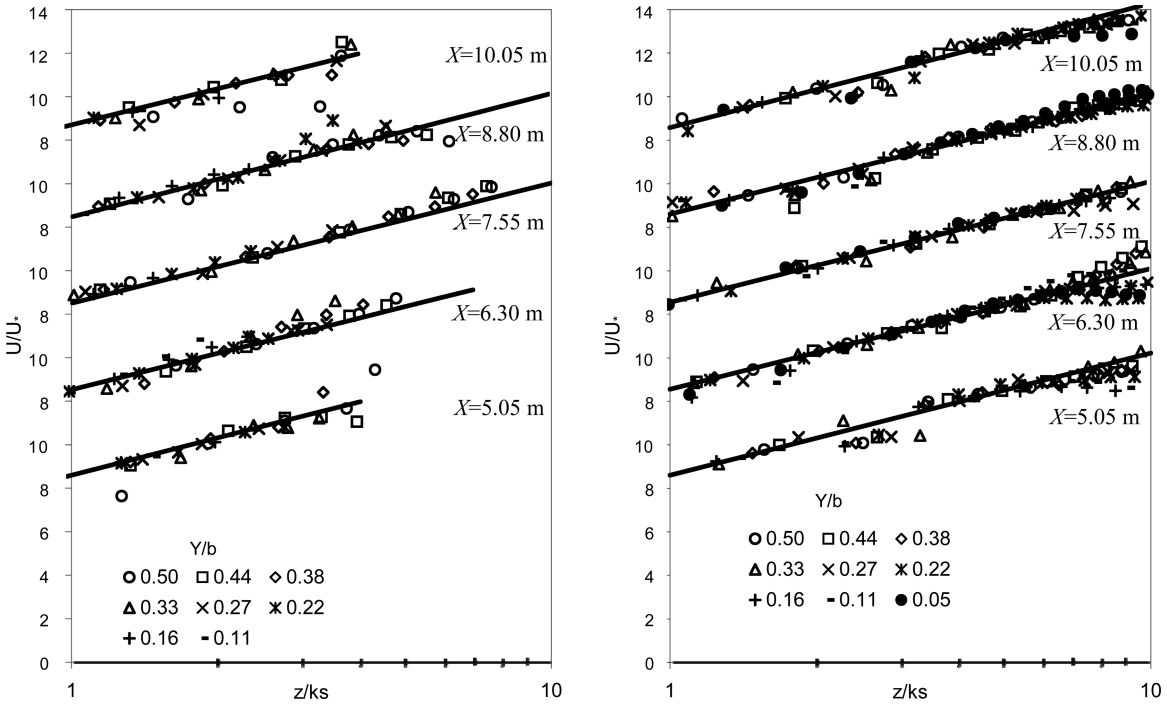

Figure 9. Streamwise velocity distribution over bed-normal rays in inner scaling: (a) low flow (CPR1) and (b) high flow (CPR2).

topographic steering and remain virtually at the same locations throughout the pool-riffle unit, in accordance with the high-flow results of *Caamaño et al*. [2012]. Vorticity plots (Figure 7) confirm the presence of three counterrotating cells at the riffles that scale with the cross-sectional flow depth. Cores of high longitudinal velocity are located in the downwelling zones between cells (at approximately one sixth and one half of the width). The described pattern at the riffle agrees with observations under flat-bed conditions in laboratory experiments [*Tamburrino and Gulliver*, 1999; *Rodríguez and García*, 2008; *Shvidchenko and Pender*, 2001] and in rivers [*Nezu and Nakagawa*, 1993]. All the mentioned cases correspond to straight reaches, where secondary currents develop as a result of turbulence anisotropy. *Rodríguez and García* [2008] also showed that the presence of vertical walls typically found in laboratory flumes and some channelized streams may reinforce this pattern. In the present experiments, the cells start more or less circular at the riffles but stretch vertically at the pool to cover the whole cross-sectional area. The secondary flow redistributes some of the momentum and energy of the main flow: downwellings transport high momentum fluid toward the bottom resulting in an incursion of the higher velocities into regions close to the bed, whereas upwellings do the opposite.

[26] It can be stated that the 3-D flow patterns in centered pool-riffle sequences appear in the form of transverse convergence-divergence and secondary currents and that the patterns are different depending on discharge conditions. The streamwise vorticity can be used to study the different mechanisms producing secondary circulation in open channels, as originally proposed by *Einstein and Li* [1958]. In steady, incompressible, constant-property flow, the mean streamwise vorticity Ω can be described using the following formula [*Perkins*, 1970]:

$$U\frac{\partial\Omega}{\partial x}+V\frac{\partial\Omega}{\partial y}+W\frac{\partial\Omega}{\partial z}=\nu\nabla^2\Omega+\Omega\frac{\partial U}{\partial x}+\underbrace{\frac{\partial U}{\partial y}\frac{\partial W}{\partial x}-\frac{\partial U}{\partial z}\frac{\partial V}{\partial x}}_{P1}+\underbrace{\frac{\partial}{\partial x}\left(\frac{\partial\overline{uw}}{\partial y}-\frac{\partial\overline{uv}}{\partial z}\right)}_{P2}+\underbrace{\frac{\partial^2}{\partial y\partial z}(w'^2-v'^2)}_{P3}+\underbrace{\left(\frac{\partial^2}{\partial y^2}-\frac{\partial^2}{\partial z^2}\right)\overline{vw}}_{P4} \tag{2}$$

[27] On physical grounds, the left-hand side of (2) is the total convection of Ω; the first term on the right-hand side is the viscous diffusion of Ω; the second represents streamwise vortex stretching; $P1$ accounts for the production of Ω by a transverse pressure gradient or body force acting on the mean shear; $P2$ is equivalent to $P1$ but at a turbulence macroscale; $P3$ is the production of Ω by turbulence anisotropy; and $P4$ represents the suppression of Ω by the Reynolds stresses $\overline{vw}$. Secondary currents originated by $P1$ are due to streamline curvature and are called Prandtl's first kind. The terms $P2$, $P3$, and $P4$ are the ones originated by turbulence, and as $P2$ is comparatively small [*Perkins*, 1970], secondary currents of Prandtl's second kind are driven by the balance between the production term $P3$ and the suppression term $P4$. The vorticity equation for only turbulence-induced secondary flow (as in the case of a flat-bed channel) can be solved for the cross section, producing

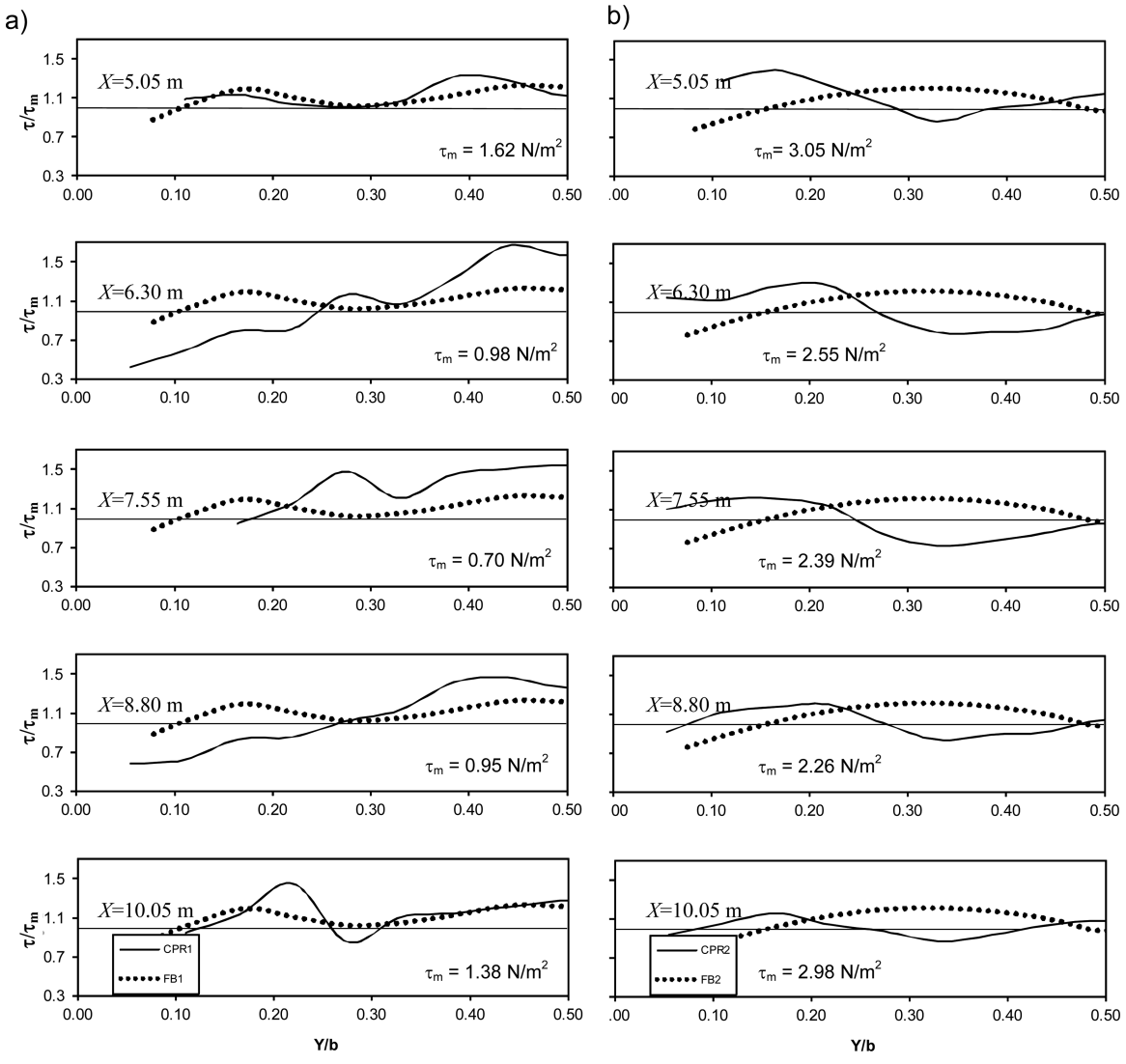

Figure 10. Cross-sectional bed shear stress distribution for (a) low flow (CPR1) and (b) high flow (CPR2). FB1 and FB2 distributions from *Rodríguez and García* [2008] are also included for comparison.

a secondary flow pattern consisting of circular counterrotating cells of diameter equal to the flow depth [*Ikeda*, 1981; *Rodríguez and García*, 2008]. The secondary flow pattern observed at the riffles during high discharge (Figures 6 and 7b) agrees with the turbulence-induced mechanism and is due to the more uniform distribution of the mean flow velocities, which results in a small $P1$ term when compared with $P3$ and $P4$. As there is no appreciable lateral topographic steering as the flow enters the pool, the counterrotating cell structure remains unchanged throughout the whole sequence.

[28] When streamline curvature is the main mechanism for the generation of secondary flow, equation (2) becomes a transport equation for the vorticity that has to be solved numerically [*Finnie et al*., 1999]. Perhaps, the most typical case for the formation of secondary currents of Prandtl's first kind (generated by the term $P1$) in open channels is flow in bends, where the principal element that drives secondary flow is the centrifugal force. The local imbalance over depth between the superelevation-generated pressure-gradient force and the curvature-induced centrifugal force results in helical motion of the time-averaged flow [*Yen*, 1965; *Yen and Yen*, 1971; *Dietrich and Smith*, 1983; *Rodríguez et al*., 2004] and a characteristic secondary circulation pattern in the cross section (Figure 1a). Another characteristic pattern of secondary circulation appears in relatively straight reaches with pool-riffle sequences [*Thompson*, 1986]. The alternation of lateral flow convergence and divergence generates streamline curvature, with superelevations and centrifugal accelerations acting similarly to flow in bends. Convergence at the pools generates superelevation over the pool deepest area with a downwelling zone that is associated with surface convergent/near-bed divergent rotating cells. At the riffles, superelevation of the water surface is located at some point between the center and the banks, and water surface is depressed at the center with an upwelling zone and an associated surface-divergent/near-bed convergent cell pattern, as shown by Figure 1b. The low-discharge pattern of the

centered pool-riffle sequence (Figures 5 and 7a) displays this characteristic behavior that results in wider circulation cells at the riffles and in cells reverting circulation direction at the pool.

5.2. Bed Shear Stresses and Self-Maintenance

[29] The distinct redistribution of momentum by topographic forcing and secondary flows has a direct impact on the bed shear stress distribution (Figures 10a and 10b). Lateral displacement of the velocity core toward the centerline is particularly important in the low-discharge case. It increases shear stresses over the cross-sectional average in the thalweg substantially, particularly at the pool entrance and to a lesser extent throughout the whole pool. No velocity core displacement is observed in the high-discharge case, and the only noticeable pattern in the pool is in fact a decrease of shear stresses at the thalweg, indicating that most of the flow momentum remains in the upper layers of the flow. On top of the general pattern of the shear stresses associated with the streamwise flow, there is an undulating effect related to the secondary circulation that produces local peaks and troughs in upwelling and downwelling regions, respectively.

[30] Integrating the values of the bed shear stresses throughout the unit, spatial averaged shear velocities of 0.03 and 0.05 m/s can be obtained for the low- and high-discharge conditions, respectively, which are slightly below the values of 0.04 and 0.06 m/s computed with the overall longitudinal water surface slope of 0.25%. Although this overall slope is the same for both discharges, the local value over the pools and riffles changes considerably generating shear velocity values (computed using the depth-slope product) of 0.055 m/s for the riffle during both CPR1 and CPR2 and of 0.03 and 0.04 m/s for the pool during CPR1 and CPR2, respectively. These local variations result in the bed shear stresses at the riffles being substantially larger than at the pool for low discharges; however, this difference is reduced as the discharge increases, as shown by Figure 11a in which the ratio of shear stresses at the pool and at the downstream riffle τ_p/τ_r have been computed using the centerline water elevations and cross-sectional depths. Cross-sectional-averaged values of τ_p/τ_r obtained by integration over the wetted perimeter of the pool and the downstream riffle are also included in Figure 11, showing a much stronger convergence for high discharge, even though the values of τ_p/τ_r remain below unity.

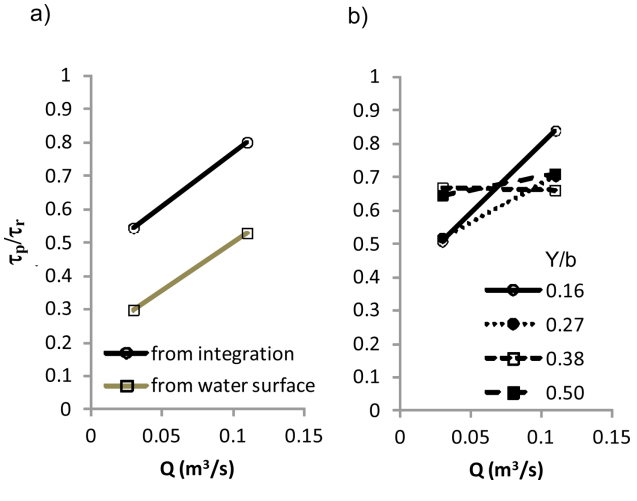

Figure 11. Ratio of pool to riffle bed shear stress as a function of discharge: (a) cross-sectional average values and (b) local values. Lines have been drawn using only two points.

[31] The change in flow behavior during low and high discharges has been reported for pool-riffle sequences, and our data provide strong quantitative indications confirming that pattern. An equalization of cross-sectional-averaged values of velocities and bed shear stresses for high discharges has been frequently observed, and in some cases, even a reversal of conditions—with velocities and shear stresses in pools surpassing those at the riffles—has occurred. In a one-dimensional, quasi-steady, fixed-bed analysis, the velocity or shear stress reversal is the only mechanism that can explain the self-maintenance of the pool-riffle sequence [*Keller*, 1971]. Reversal in a cross-sectional-averaged sense has been observed or predicted in a limited number of cases, and therefore, alternative explanations for self-maintenance have been attempted focusing on local rather than averaged conditions. Figure 11a shows that neither equalization nor reversal occurred in the experiments using cross-sectional-averaged values of bed shear stress. The detailed measurements presented in this paper can be used to test local reversal conditions trends by comparing the pool to downstream riffle shear stress ratio τ_p/τ_r at different Y/b positions for the two different discharges, as shown in Figure 11b. For the low-discharge case, in which important lateral flow expansion occurred in going from the pool to the riffle, the values used at the riffle were laterally shifted toward the bank by 0.05 m with respect to the corresponding values at the pool (e.g., the value of τ_p at $Y = 0.45$ was divided by the value of τ_r at $Y = 0.4$). Figure 11b shows that the local reversal trends are more pronounced close to the bank but less marked (reduced steepness of the trend line) near the centerline of the cross section when compared with the cross-sectional average reversal trend (Figure 11a). In that sense, if it is assumed that most sediment is transported through the central path for the particular geometry studied here, the results do not support the idea that local flow variations improve the self-maintenance characteristics of the pool-riffle sequence.

[32] From the previous analysis, it is clear that the proposed design has very limited capabilities to self-maintain itself, as it produces higher shear stresses at the riffles for both low- and high-discharge conditions. Values of relative competence τ_p/τ_r of 0.8 (cross-sectional average) or 0.7 (local) for the high-flow condition are not indicative of self-maintenance unless some other mechanisms are considered. The current design is not likely to generate strong turbulent coherent structures that enhance relative competence and self-maintenance; however, the bed sediment composition may have important effects due to resistance to erosion [*Clifford*, 1993; *Sear*, 1996] or differential roughness [*Carling and Wood*, 1994]. Moreover, if the quasi-steady and fixed-bed assumptions are relaxed and sediments of different sizes are considered, the requirements for self-maintenance are not as stringent [*de Almeida and Rodríguez*, 2011, 2012]. Sediment transport reversal conditions that lead to self-maintenance can be achieved with values of τ_p/τ_r as low as 0.3; however, they are very common for τ_p/τ_r values of 0.6 or greater due to the combined effect of mean flow

unsteadiness, differential sediment mobility, and bed elevation changes at the riffles [*de Almeida and Rodríguez*, 2011, 2012]. Figure 11 shows that the high-discharge τ_p/τ_r values for the central pool-riffle sequence can be as high as 0.8, which would imply that the design may be capable of self-cleaning during bankfull discharges. Of course this would be dependent on the differential sediment mobility between pool and riffle, and thus, specific tests should be conducted to assert this issue. Interestingly, *Rhoads et al*. [2011] presented the successful implementation of the present design for a limited load stream (the WFNBCR), but did not recommend the present design for a stream with high bedload (mainly sand) transport and proposed a modification to the design with a more constricted pool to enhance self-maintenance.

5.3. Hydrodynamic Variability

[33] Besides being able to self-maintain, pool-riffle sequences used in stream restoration projects are expected to provide an increased level of flow variability necessary to support a rich ecological environment. Measures of flow variability can be obtained by quantifying the bed shear stress variation with respect to its cross-sectional value τ/τ_m (Figure 10) and with respect to its spatial average over the whole unit $\tau/\langle\tau\rangle$ or shear stress footprint as presented in Figure 12. In Figure 12, $\langle\tau\rangle$ values of 1.01 and 2.55 N/m^2 for the low- and high-discharge conditions, respectively, have been computed by integration of local the local τ values of Figure 10 over the unit. It must be noted that these estimates compare quite well with the values of 0.9 and 2.5 N/m^2 obtained from the $\langle U^*\rangle$ estimates of Table 1 based on the overall reach slope. In that respect, they provide an indirect confirmation that the methodology used for the bed shear stress computation is appropriate.

[34] With respect to cross-sectional variability, Figure 10 shows that the low-discharge case presents maximum τ/τ_m values that are larger in the pool (1.5 to 1.7) than in the riffle (1.3 to 1.5), whereas the high-discharge case displays an almost uniform value (1.2 to 1.4) that is smaller than in the low-discharge case. The same difference in the level of concentration of local values of the bed shear stress is observed in the footprint of Figure 12, with maximum $\tau/\langle\tau\rangle$ values of 1.8 and 1.3 for the low- and high-discharge cases, respectively. It is interesting to note that results on the same experimental facility over a flat bed composed of the same bed material (Table 1) [*Rodríguez and García*, 2008] produced τ/τ_m values of 1.2, comparable with the high-discharge-centered pool-riffle.

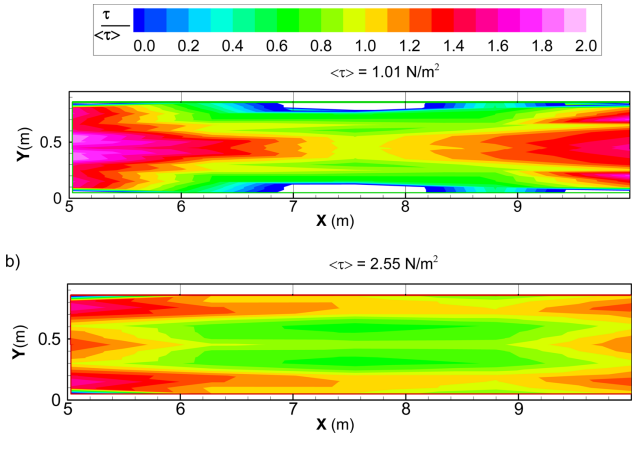

Figure 12. Bed shear stress spatial distribution or footprint: (a) low flow (CPR1) and (b) high flow (CPR2).

[35] Another measure of flow variability can be obtained by looking at the velocity concentration areas (jets), which are quite evident in Figures 5 and 6. When scaled with the reach average velocity (Table 1), the highest $U/\langle U\rangle$ value for the low flow is 1.6, substantially higher than that for the high-discharge case, which is only about 1.3. The latter value is close to the flat bed value of 1.25 (Table 1) [*Rodríguez and García*, 2008] for both high and low discharges.

[36] The last two paragraphs show that although the low-discharge case has a more variable spatial distribution due to a more pronounced effect of the topography over the flow patterns, the level of spatial flow variability for the high-discharge case is practically the same as in a flat-bed situation. Consequently, for the particular geometry studied in this paper, the spatial variability in the flow patterns typically associated with pool-riffle sequences, and frequently linked to their ecological value, is only observed for low discharges.

6. Conclusions

[37] Detailed 3-D velocity measurements carried out on a centered pool-riffle sequence designed for restoring a channelized stream have allowed the reconstruction of flow patterns for two different discharge conditions, corresponding approximately to the 1- and 2-year return floods. The design incorporated basic geomorphological features of natural pool-riffle sequences, and the analysis focused on the general characteristics of the flow patterns, the self-maintenance capabilities of the design, and the flow variability added to the original channelized stream by the new structures.

[38] With respect to the general flow patterns, a discharge-dependent organization of the flow was observed. The lower discharge displayed a strong effect of the topography, which generated high-velocity cores at the riffle associated with the alternation of lateral convergence and divergence. The velocity cores moved toward the center of the pool due to lateral convergence. Secondary circulation cells displayed a surface-divergent/near-bed convergent pattern at the center of the riffle, which was replaced by a surface-convergent/near-bed divergent pattern at the pool center, as observed in natural pools and riffles and originated by streamline curvature. It must be noted, however, that stronger transverse flow patterns are found in natural pools [*MacVicar and Rennie*, 2012]. The higher discharge case was more uniform, with velocity cores and secondary circulation showing only minor effects of the topography. High-velocity cores and associated secondary circulation cells remained at the same transverse locations throughout the whole structure, with the cells stretching vertically to occupy most of the cross section at the pool. This secondary circulation pattern has been associated with turbulence anisotropy.

[39] It was found that reversal conditions in bed shear stresses at pool and riffle sections did not occur for the two discharges tested, only a convergence of the values with increasing discharge. Reversal of the relative magnitude of

pool and riffle shear stresses for high discharges has been observed in natural pools and riffles and associated with self-maintenance of the structures. The level of convergence observed for this particular design could only generate self-maintenance conditions if additional factors were considered, like unsteadiness effects on the differential mobility of the sediment in pools and riffles [*deAlmeida and Rodríguez*, 2011, 2012]. The level of convergence did not increase when local rather than cross-sectional values were analyzed.

[40] Spatial flow variability was assessed by looking at maximum values of velocities and bed shear stresses and comparing them with the reference flat-bed condition. The lower discharge displayed larger variability than the flat-bed situation; however, the higher discharge generated a low level of variability comparable with the values obtained over a flat bed. At least for the pool-riffle design being tested in this paper, the spatial flow variability sought after for ecological reasons could only be verified for the lower discharge case.

[41] **Acknowledgments.** Partial financial support was provided by the project "Development of an Integrated Scientific and Technological Framework for Stream Naturalization," grant 98-NCERQA-M1, U.S. Environmental protection Agency. The comments of three anonymous reviewers and the Associate Editor greatly helped to improve the manuscript.

References

Andrews, E. D. (1979), *Scour and Fill in a Stream Channel, East Fork River, Western Wyoming*, p. 47, United States Government Printing Office, Washington, D. C.

Bathurst, J. C. (1982), Channel bars in gravel-bed rivers [Discussion], in *Gravel-Bed Rivers*, edited by R. D. Hey, J. C. Bathurst, and C. R. Thorne, pp. 330–331, John Wiley, Chichester, U. K.

Bhowmik, N. G., and M. Demissie, (1982), Bed material sorting in pools and riffles, *J. Hydraul. Div. Am. Soc. Civ. Eng.*, *108*(HY10), 1227–1231.

Booker, D. J., D. A. Sear, and A. J. Payne (2001), Modeling three-dimensional flow structures and patterns of boundary shear stress in a natural pool-riffle sequence, *Earth Surf. Processes Landforms*, *26*, 553–576.

Caamaño, D., P. Goodwin, and J. M. Buffington (2012), Flow structure through pool-riffle sequences and a conceptual model for their sustainability in gravel-bed rivers, *River Res. Appl.*, *28*, 377–389, doi:10.1002/rra.1463.

Carling, P. A., and N. Wood (1994), Simulation of flow over pool-riffle topography: A consideration of the velocity reversal hypothesis, *Earth Surf. Processes Landforms*, *19*, 319–332.

Cao, Z., P. A. Carling, and R. Oakley (2003), Flow reversal over a natural pool-riffle sequence: A computational study, *Earth Surf. Processes Landforms*, *28*, 689–705.

Clifford, N. J. (1993), Differential bed sedimentology and the maintenance of riffle-pool sequences, *Catena*, *20*, 447–468.

Clifford, N. J., and K. S. Richards (1992), The reversal hypothesis and the maintenance of riffle-pool sequences: A review and field appraisal, in *Lowland Floodplain Rivers: Geomorphological Perspectives*, edited by P. A. Carling and G. E. Petts, pp. 43–70, John Wiley, Chichester, U. K.

Clifford, N. J., and J. R. French (1993), Monitoring and analysis of turbulence in geophysical boundaries: Some analytical and conceptual issues, in *Perspectives on Flow and Sediment Transport*, edited by N. J Clifford, J. R. French, and J. Hardisky, pp. 93–120, John Wiley, Chichester, U. K.

de Almeida, G. A. M., and J. F. Rodríguez (2011), Understanding pool-riffle dynamics through continuous morphological simulations, *Water Resour. Res.*, *47*, W01502, doi:10.1029/2010WR009170.

de Almeida, G. A. M., and J. F. Rodríguez (2012), Spontaneous formation and degradation of pool-riffle morphology and sediment sorting using a simple fractional transport model, *Geophys. Res. Lett.*, *39*, L06407, doi:10.1029/2012GL051059.

Dietrich, W. E. (1987), Mechanics of flow and sediment transport in river bends, in *River Channels: Environment and Process*, edited by K. S. Richards, pp. 179–227, Basil Blackwell, Oxford, U. K.

Dietrich, W. E., and J. D. Smith (1983), Influence of the point bar on flow through curved channels, *Water Resour. Res.*, *19*(5), 1173–1192.

Einstein, H. A., and H. Li (1958), Secondary currents in straight channels, *Trans. Am. Geophys. Union*, *39*, 1085–1088.

Finnie, J., B. Donnell, J. Letter, and R. Bernard (1999), Secondary flow correction for depth averaged flow calculations, *J. Eng. Mech.*, *125*(7), 109–124.

Gilbert, G. K. (1914), The transportation of debris by running water, *U.S. Geol. Surv. Prof. Pap., 86*.

Hart, D. D., and C. M. Finelli (1999), Physical-biological coupling in streams: The pervasive effects of flow on benthic organisms, *Annu. Rev. Ecol. Syst.*, *30*, 363–395.

Ikeda, S. (1981), Self forced straight channels in sandy beds, *J. Hydraul. Div. Am. Soc. Civ. Eng.*, *107*(HY4), 389–406.

Keller, E. A. (1971), Areal sorting of bed-load material: The hypothesis of velocity reversal, *Geol. Soc. Am. Bull.*, *82*, 753–756.

Keller, E. A. (1972), Development of alluvial stream channels: A five stage model, *Geol. Soc. Am. Bull.*, *83*, 1531–1536.

Keller, E. A., and W. N. Melhorn (1978), Rhythmic spacing and origin of pools and riffles, *Geol. Soc. Am. Bull.*, *89*, 723–730.

Lane, E. W., and W. M. Borland (1954), River-bed scour during floods, *Trans. Am. Soc. Civ. Eng.*, *119*, 1069–1079.

Lisle, T. E. (1979), A sorting mechanism for a riffle-pool sequence, *Geol. Soc. Am. Bull.*, *90*, 1142–1157.

López, F. M. L. (2006), Flow characteristics in pool-riffle structures under the presence of vegetation, M.S. thesis, Dept. of Civil and Environ. Eng., Univ. of Illinois at Urbana-Champaign, Ill.

Lundgren, H., and I. G. Jonsson (1964), Shear and velocity distribution in shallow channels, *J. Hydraul. Div. Am. Soc. Civ. Eng.*, *90*(HY1), 1–21.

MacVicar, B. J., and A. G. Roy (2007a), Hydrodynamics of a forced riffle pool in a gravel bed river: 1. Mean velocity and turbulence intensity, *Water Resour. Res.*, *43*, W12401, doi:10.1029/2006WR005272.

MacVicar, B. J., and A. G. Roy (2007b), Hydrodynamics of a forced riffle pool in a gravel bed river: 2. Scale and structure of coherent turbulent events, *Water Resour. Res.*, *43*, W12402, doi:10.1029/2006WR005274.

MacVicar, B. J., and C. D. Rennie (2012), Flow and turbulence redistribution in a straight artificial pool, *Water Resour. Res.*, *48*, W02503, doi:10.1029/2010WR009374.

MacWilliams, M. L., Jr., J. M. Wheaton, G. B. Pasternack, R. L. Street, and P. K. Kitanidis (2006), Flow convergence routing hypothesis for pool-riffle maintenance in alluvial rivers, *Water Resour. Res.*, *42*, W10427, doi:10.1029/2005WR004391.

Nelson, J. M., S. R. McLean, and S. R. Wolfe (1993), Mean flow and turbulence fields over two-dimensional bed forms, *Water Resour. Res.*, *29*, 3935–3953.

Nelson, J. M, R. L. Shreve, S. R. McLean, and T. G. Drake (1995), Role of near-bed turbulence structure in bed transport and bed form mechanics, *Water Resour. Res.*, *31*, 2071–2086.

Newbury, R., and M. Gaboury (1993), Exploration and rehabilitation of hydraulic habitats in streams using principles of fluvial behavior, *Freshwater Biol.*, *29*, 195–210.

Nezu, I., and H. Nakagawa (1993), *Turbulence in Open Channel Flows*, A. A. Balkema, Rotterdam, Netherlands.

Nikora, V. I., D. G. Goring, and B. J. Biggs (2002), Some observations of the effects of micro-organisms growing on the bed of an open channel on the turbulence properties, *J. Fluid Mech.*, *450*, 317–341.

O'Connor, J. E., R. H. Webb, and V. R. Baker (1986), Paleohydrology of pool-and-riffle pattern development, Boulder Creek, Utah, *Geol. Soc. Am. Bull.*, *97*, 410–420.

Parker, G. (1978), Self-formed straight rivers with equilibrium banks and mobile bed. Part 2. The gravel river, *J. Fluid Mech.*, *89*, 127–146.

Perkins, H. J. (1970), The formation of streamwise vorticity in turbulent flow, *J. Fluid Mech.*, *44*, 721–740.

Petit, F. (1987), The relationship between shear stress and the shaping of the bed of a pebble-loaded river La Rulles-Ardelle, *Catena*, *14*, 453–468.

Pizzuto, J. (1991), A numerical model for calculating the distribution of the velocity and boundary shear stress across irregular straight open channels, *Water Resour. Res.*, *27*(9), 2457–2466.

Rhoads, B. L., and M. R. Welford (1991), Initiation of river meandering, *Prog. Phys. Geogr.*, *15*, 127–156.

Rhoads, B. L., M. H. García, J. F. Rodríguez, F. A. Bombardelli, J. D. Abad, and M. D. Daniels (2008), Methods for evaluating the geomorphological performance of naturalized rivers: Examples from the Chicago metropolitan area, in *Uncertainty in River Restoration*, edited by D. Sears and S. Darby, pp. 209–228, John Wiley, Chichester, U. K.

Rhoads, B. L., F. L. Engel, and J. D. Abad (2011), Pool-riffle design based on geomorphological principles for naturalizing straight channels, in *Stream Restoration in Dynamic Fluvial Systems: Scientific Approaches, Analyses, and Tools*, edited by A. Simon, S. J. Bennett, and J. M. Castro, pp. 367–384, AGU, Washington, D. C., doi:10.1029/2010GM000979.

Rodríguez, J. F. (2004), Mean flow and turbulence characteristics of pool-riffle structures in low-gradient streams, Ph.D. dissertation, Dept. of Civ. and Environ. Eng., Univ. of Illinois at Urbana-Champaign, Ill.

Rodríguez, J. F., and M. H. García (2008), Laboratory measurements of 3-D flow patterns and turbulence in straight open channels with rough bed, *J. Hydraul. Res.*, *46*(4), 454–465, doi:10.3826/jhr.2008.2994.

Rodríguez, J. F., B. Belby, F. A. Bombardelli, C. M. García, B. L. Rhoads, and M. H. García (2001), Numerical and physical modeling of pool-riffle sequences for low-gradient urban streams, paper presented at InternationalSymposium on Environmental Hydraulics, IAHR, Tempe, Ariz.

Rodríguez, J. F., F. A. Bombardelli, M. H. García, K. Frothingham, B. L. Rhoads, and J. D. Abad (2004), High-resolution numerical simulation of flow through a highly sinuous river reach, *Water Resour. Manage.*, *18*(3), 177–199.

Rodríguez, J. F., M. H. García, F. A. Bombardelli, J. M. Guzmán, B. L. Rhoads, and E. Herricks (2000), Naturalization of urban streams using in-channel structures, paper presented at Joint Conference on Water Resources Engineering and Water Resources Planning and Management, ASCE, Minneapolis, Minn.

Sear, D. A. (1996), Sediment transport in pool-riffle sequences, *Earth Surf. Processes Landforms*, *21*, 241–262.

Shimizu, Y. (1989), Effects of lateral shear stress in open-channel flow, *River Hydraul. and Hydrol. Lab. Rep.*, Civil Engineering Research Institute, Hokkaido Development Bureau.

Shvidchenko, A. B., and G. Pender (2001), Macroturbulent structure of open-channel flow over gravel beds, *Water Resour. Res.*, *37*(3), 709–719.

Smart, G. M. (1999), Turbulent velocity profiles and boundary shear in gravel bed rivers, *J. Hydraul. Eng.*, *125*(2), 106–116.

Song, T., and Y. M. Chiew (2001), Turbulence measurement in nonuniform open-channel flow using acoustic Doppler velocimeter (ADV), *J. Eng. Mech.*, *127*(3), 219–231.

Tamburrino, A., and J. S. Gulliver (1999), Large flow structures in a turbulent open channel flow, *J. Hydraul. Res.*, *37*(3), 363–380.

Teleki, P. G. (1972), Areal sorting of bed-load material: The hypothesis of velocity reversal [Discussion], *Geol. Soc. Am. Bull.*, *83*, 911–914.

Thompson, A. (1986), Secondary flows and the pool-riffle unit: A case study of the processes of meander development, *Earth Surf. Processes Landforms*, *11*, 631–641.

Thompson, D. M. (2002), Channel bed scour with high versus low deflectors, *J. Hydraul. Eng.*, *128*(6), 640–642.

Thompson, D. M. (2011), The velocity-reversal hypothesis revisited, *Prog. Phys. Geogr.*, *35*, 123, doi:10.1177/0309133310369921.

Thompson, D. M., and E. E. Wohl (2009), The linkage between velocity patterns and sediment entrainment in a pool-riffle unit, *Earth Surf. Processes Landforms*, *34*, 177–192.

Thompson, D. M., E. E. Wohl, and R. D. Jarret (1999), Velocity reversals and sediment sorting in pools and riffles controlled by channel constrictions, *Geomorphology*, *27*, 229–241.

Wade, R. J., B. L. Rhoads, J. F. Rodríguez, M. Newell, D. Wilson, E. Herricks, F. A. Bombardelli, and M. H. García (2002), Integrating science and technology to support stream naturalization near Chicago, Illinois, *J. Am. Water Resour. Assoc.*, *38*(4), 931–945.

Yang, S. Q., and A. T. Chow (2008), Turbulence structures in non-uniform flows, *Adv. Water Resour.*, *31*(10), 1344–1351.

Yen, B. C. (1965), Characteristics of subcritical flow in a meandering channel, *Report*, IIHR, Univ. of Iowa, Iowa.

Yen, C., and B. C. Yen (1971), Water surface configuration in channel bends, *J. Hydraul. Div. Am. Soc. Civ. Eng.*, *97*, 303–321.